EFFECTS OF THE FAN - HEAT EXCHANGER INTERACTION ON THE NOISE EMISSIONS OF HEAT PUMPS: EXPERIMENTAL AND NUMERICAL STUDIES

Sebastian WAGNER[1], Jens ROHLFING[2]

[1] *Institute for Acoustics and Building Physics IABP, University of Stuttgart, 70569 Stuttgart, Germany*

[2] *Fraunhofer Institute for Building Physics IBP, 70569 Stuttgart, Germany*

SUMMARY

In this study, the interaction between a fan and two types of heat exchangers is investigated experimentally, using an adjustable mock-up closely resembling the outdoor unit of a heat pump. Several aerodynamic and acoustic investigations have been conducted. The velocity field at the front of the heat exchanger is measured manually with an impeller anemometer. The velocity field between the heat exchanger and the fan is analyzed using the Laser-Doppler Velocimetry. Furthermore, a simplified geometrical model of the experimental setup is used to numerically analyze the airflow through the heat exchanger - fan assembly. Preliminary simulation results generated with this simplified model are presented and compared to the experimental results.

INTRODUCTION

Heat pumps are proven to be an efficient and environment-friendly key technology to reduce CO_2 emissions [1]. Hence, modern electrically driven heat pumps have become an attractive alternative to conventional heating systems. Today, an increasing number of heat pumps is installed, especially in dense urban areas [2]. Therefore, the noise emissions from heat pumps are of increasing relevance. Research on the acoustic behavior of heat pumps with respect to noise control and noise perception is now a major topic in the research and development efforts of heat pump manufacturers. The publicly funded German research project “WAMS” is investigating the noise emissions of heat pumps. One of the main noise sources of heat pump outdoor units are the fans. In a heat pump, the fan is used to move ambient air across a heat exchanger (HEX), which transfers the thermal energy of the air to a cooling agent. There are various possible HEX types and HEX-fan arrangements, which can be used when designing an outdoor unit. In order to investigate the effect of the interaction between HEX and a fan on the acoustic emissions, experimental studies have been conducted with a simplified test setup. This experimental setup allows the systematic investigation

of various HEX-fan configurations, e.g., variations of distances and the angles of the HEX, as well as different HEX types, such as classical round tube (RT) and microchannel (MC) HEXs. As presented in [3], a HEX on the suction side of the fan can have a significant influence on the sound power level at the blade passing frequency (BPF) and its higher harmonics. Studies on the velocity flow field between the HEX and the fan have been conducted using Laser-Doppler Velocimetry. In the next section, the heat pump mockup and the HEX-fan configurations used in this study are explained, and the experimental results are presented and discussed. Furthermore, a simulation model with a simplified geometry is introduced, which is used to perform numerical simulations. The simulations are performed with the open source software OpenFOAM® [4]. In addition to previously presented simulations [3], a more detailed fan geometry is used in the model. A comparison between the measured and simulated pressure losses is presented.

HEAT PUMP MOCK-UP AND MEASUREMENT SETUP

Heat pump mock-up

In collaboration with the Fraunhofer Institute for Solar Energy Systems ISE, a heat pump mock-up has been designed to investigate the interaction between HEX and fan in an outdoor unit of a heat pump. As shown in Figure 1, with this mock-up, various HEX-fan configurations can be realized and investigated experimentally in terms of noise emissions and aerodynamics. In the experimental studies, the influence of various HEX types and the HEX-fan distance on the sound power level and the radiation characteristic have been investigated [3]. To get a better understanding of the parameters that may influence the sound power level at the BPF and its higher harmonics, the velocities on the inlet side of the heat pump mock-up have been measured for the configurations with the HEX installed, as shown in Figure 1 b). Figure 1 c) shows the measurement grid with 90 positions used for the velocity measurements. The flow velocity has been measured on the suction side directly in front of the RT-HEX at a distance of about 2 cm using an impeller anemometer. For these measurements, the perimeter of the HEX was carefully sealed with a permanent plastic sealant to avoid unintentional inflow through the corners and edges. The measurements have been performed for fan speeds of 635 rpm and 1060 rpm, corresponding to 60 % and 100 % of the maximum fan speed.

a) b) c)

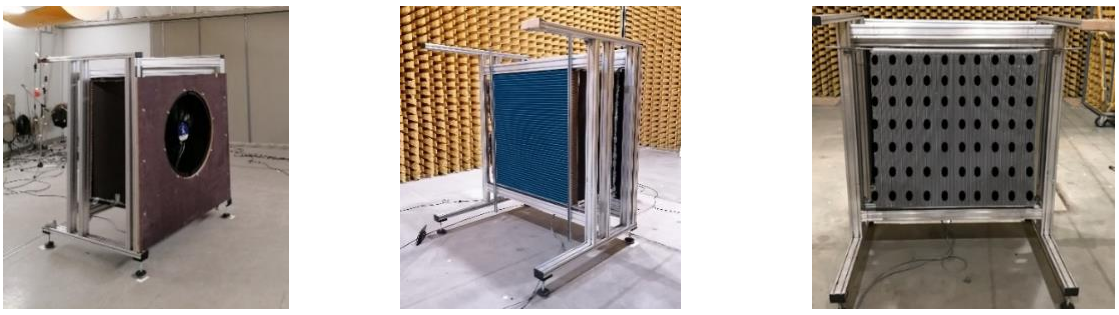

Figure 1: Pictures of the heat pump mockup; a) pressure side view of the mock-up in the reverberation room, b) suction side view of the mock-up in the semi-anechoic room and c) suction side view with indication of the measurement points for the flow velocity.

Laser-Doppler Velocimetry

In addition to the noise investigations, the flow field inside the heat pump mock-up has been investigated using the Laser-Doppler Velocimetry (LDV) [5, 6]. The investigations have been performed with a two-laser system from the company ILA R&D GmbH. Figure 2 a shows the measurement setup for the experimental study: 1) aerosol generator; 2) traversing system with the laser; 3) aerosols outlet. With the traversing system, the laser can be moved to reach all the

measurement points in the selected measurement plane. For these measurements, the heat pump mock-up had to be modified. A part of the side plate was replaced by a double antireflective glass to reduce the back scatter of the light. Figure 2 b schematically shows the top view of the heat pump mock-up with the position of the measurement grid chosen for the LDV measurements. The distance between the measurement position and the fan duct was Δx = 6 cm. Hence, it was possible to investigate the flow field for several HEX-fan distances [3]. Figure 2 c, the radial measurement grid with nearly 290 measurement positions is visualized. A detailed description of the LDV measurement principle can be found in [5, 6].

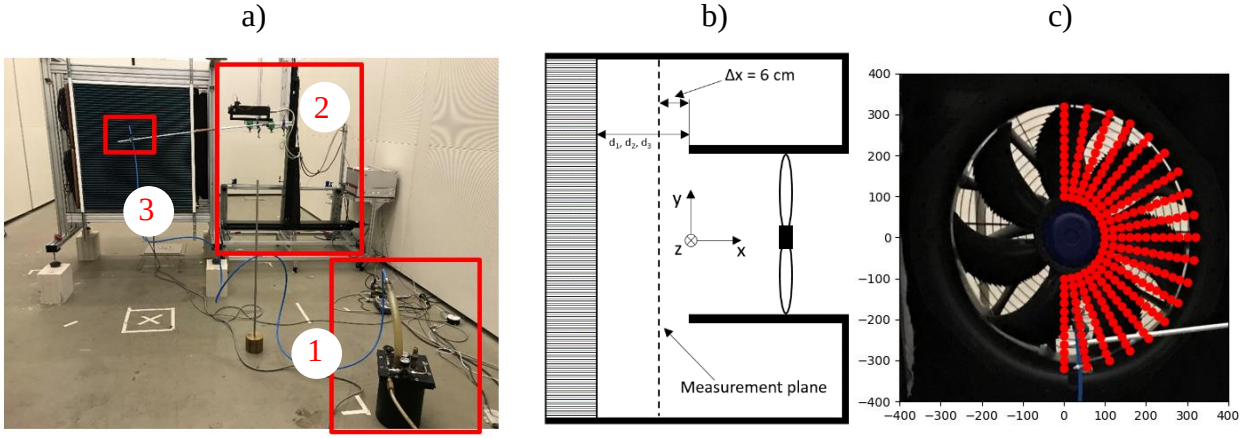

Figure 2: a) Picture of the measurement setup for the LDV flow field analysis. b) Sketch of the heat pump mock-up cross section with position of the measurement plane; c) visualization of the radial measurement grid.

EXPERIMENTAL RESULTS

Acoustic characterization

The acoustic measurements on the heat pump mock-up presented in this section have been conducted in the reverberation room at the Fraunhofer IBP. The sound power levels have been determined according to the reverberation room method described in DIN EN ISO 3741 [7]. Figure 3 shows the 1/3 octave band sound power spectra for different HEX-fan distances, d_1 = 10 cm, d_2 = 20 cm and d_3 = 40 cm, and fan speeds of 635 rpm and 1060 rpm.

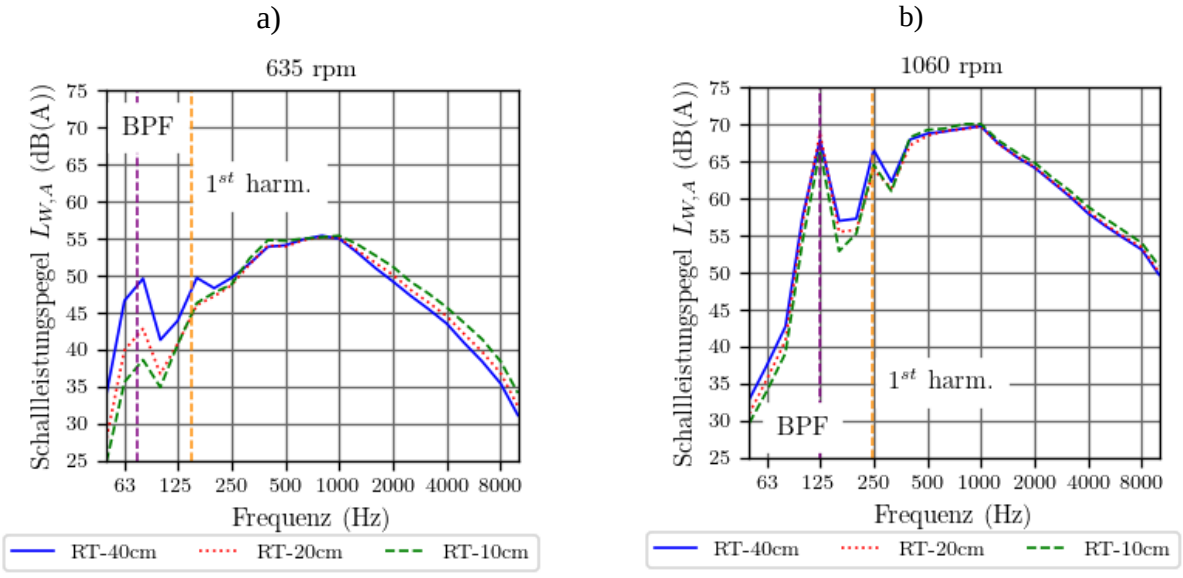

Figure 3:Sound power spectra depending on the HEX-fan distance a) 635 rpm and b) 1060 rpm [3].

By changing the fan speed from 635 rpm to 1060 rpm, the A-weighted sound power levels are increased by about 25 dB. The results show that for a fan speed of 635 rpm, the sound power levels around the BPF and its higher harmonics decrease when the HEX-fan distance is reduced[3]. For a fan speed of 1060 rpm, the BPF and its higher harmonics shift towards higher frequencies proportional to the rising fan speed. However, the results for a fan speed of 1060 rpm show only a small effect of the HEX-fan distance on the sound power levels around the BPF and its higher harmonics. To get a better understanding on which parameters influence the sound power levels at the BPF, additional flow velocity measurements have been conducted.

Flow field between HEX and fan

Figure 4 shows the velocities and the turbulence intensities for the distances d_1 and d_3 at 635 rpm, measured using the LDV. The results show increasing flow velocities for increasing HEX-fan distances. The averaged flow velocity $\bar{v}_x$ is increased by nearly 30 % by changing the distance from d_1 to d_3, which consequently results in higher flow rates. Also, the flow fields become more homogeneous with increasing HEX-fan distances. As expected, the lowest flow velocities in the measurement plane occur near the fan hub.

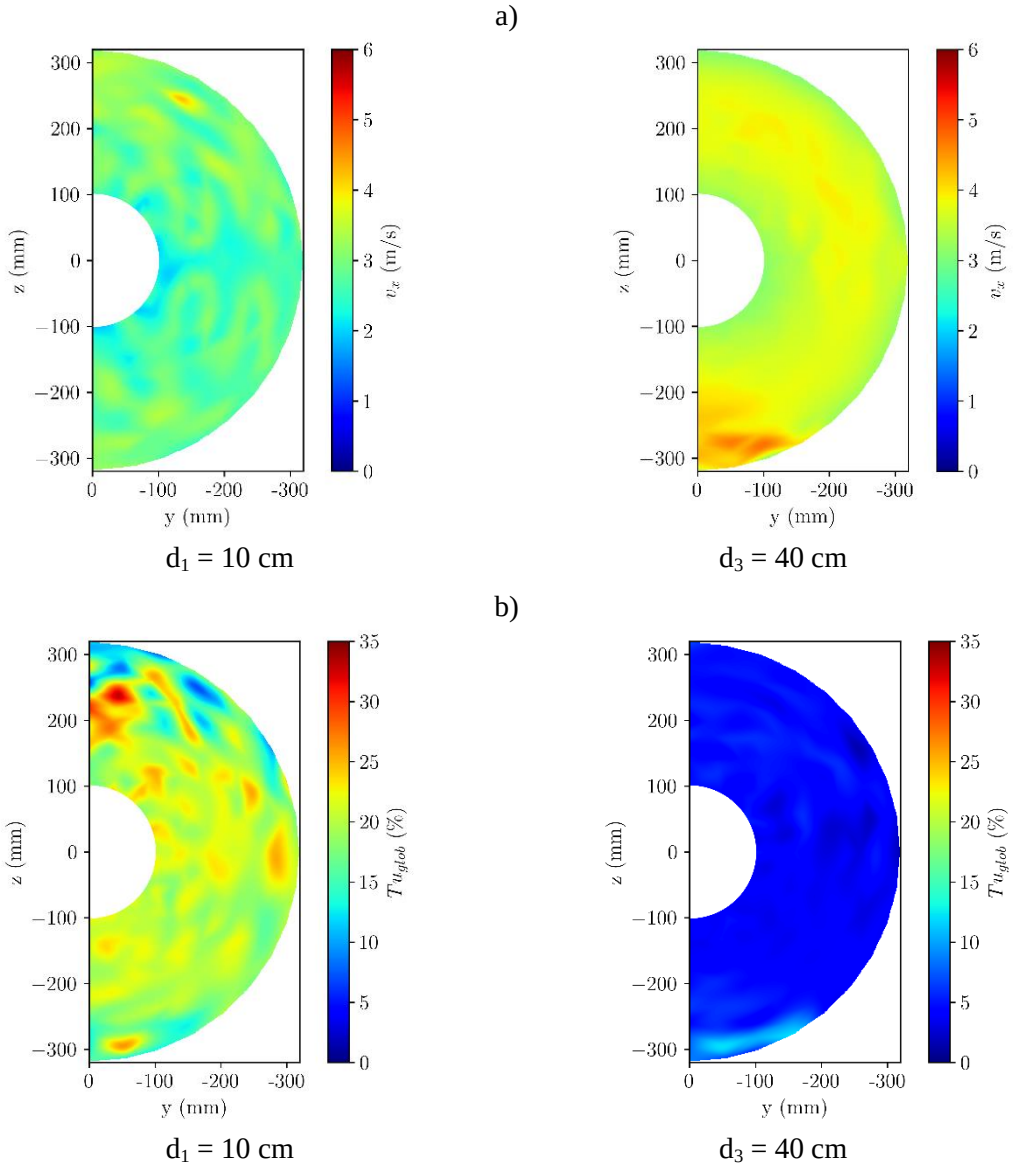

Figure 4: a) Measured flow velocities v_x and b) turbulence intensity Tu_{glob} depending on the HEX-fan distance.

In Figure 4 b), the turbulence intensity for the HEX-fan distances d_1 and d_3 is visualized. The results show that the turbulence intensity is decreasing with increasing HEX-fan distance. As discussed in [8, 9], different turbulent inflow conditions can have an influence on the overall sound power level. For the investigated configurations, the presented aerodynamic and acoustic measurements cannot fully confirm this thesis, since it was found that with decreasing turbulent inflow, the sound power level around the BPF decreases. The analysis of the LDV experimental data is still ongoing. In the near future, investigations on the flow field for additional fan speeds and a HEX-fan distance of d_2 = 20 cm will be performed. For the LDV measurements, various measurement grids have been used, e.g., a Cartesian mesh, for a more direct comparison between the experimental results and the simulations. This analysis is also still ongoing and will be presented in future publications.

Flow field characterization on the heat exchanger inlet

Figure 5 shows the interpolated flow velocity distributions in the main flow direction v_x, measured on the suction side in front of the RT-HEX for different HEX-fan distances. For these measurements, a measurement grid with 90 positions distributed across the HEX area, as shown in Figure 1 c), has been used. The size of the HEX is about 0.9 m^2 with a height of 1,0 m and a width of 0.9 m. Figure 5 a)-c) show the measured flow velocity field for a fan speed of 635 rpm, and Figure 5 d)-f) show the velocity field for a fan speed of 1060 rpm. For a HEX-fan distance d_1, the results for both fan speeds roughly show the round contours of the fan inlet nozzle inside the heat pump mock-up. As the HEX-fan distance increases, the flow velocities across the measurement grid are more evenly distributed. For all HEX-fan combinations, the lowest flow velocities are observed around the upper and lower part of the measurement grid. For higher fan speeds, the lowest flow velocities are measured at the top edge of measurement grid. For a HEX-fan distance d_3, the maximum flow velocities are measured closer to the lower left side of the measurement grid.
In Figure 5, the overall averaged flow velocities for all measurement setups are also stated. The averaged flow velocities have been calculated below according to Eqn. (1):

$$\dot{V} = A_{HEX} \cdot \frac{1}{n} \sum_{1}^{n} v_i \,. \tag{1}$$

For fan speeds of 635 rpm and 1060 rpm, the results for HEX-fan distances of d_1 = 10 cm and d_2 = 20 cm give identical averaged flow velocities of v_x = 1.6 m/s and v_x = 2.9 m/s, respectively. As the HEX-fan distance is increased to d_3 = 40 cm, the average flow velocities increase by 25 % at 635 rpm and by 7 % at 1060 rpm to v_x = 2.0 m/s and v_x = 3.1 m/s, respectively. Hence, to reach larger flow rates, larger HEX-fan distances seem to be beneficial. As higher flow rates are likely to result in an increased heat transfer in the HEX, this may have a direct effect on the Coefficient of Performance (COP) of a heat pump. The larger change in the flow velocity, depending on the HEX-fan distance, was measured for 635 rpm compared to 1060 rpm. This phenomenon may also be the reason for the higher HEX-fan distance dependency of the sound power levels around the BPF and its higher harmonics.
Figure 6 shows the flow rates depending on the fan speed and the distance between the HEX and the fan. The triangles indicate the flow rates for d_3, the crosses mark the results for d_2 = 20 cm, and the points indicate the flow rates for d_1 = 10 cm. For each of the investigated HEX-fan distance, the results show an approximately linear rise in the flow rate with increasing fan speed. The largest flow rate at a fan speed of 423 rpm (40 %) is measured for d_1. For the other fan speeds, the largest flow rates are measured for d_3. The largest increases in the flow rates for different HEX-fan distances are found for a fan speed of 635 rpm (60 %), which corresponds to 18.4 %. For a fan speed of 848 rpm (80 %), the maximum difference in the flow rate is 11.5 %.

a)

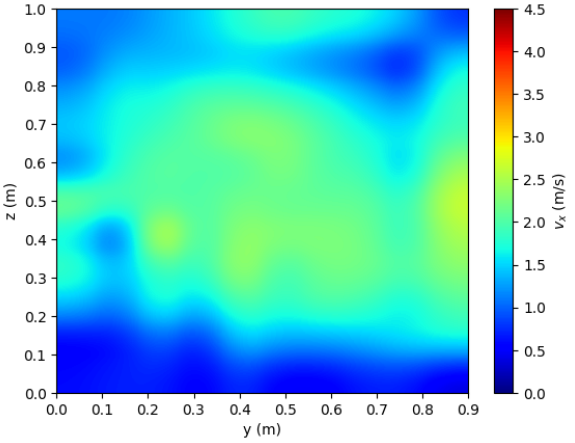

$\bar{v}_x = 1.6\ m/s$; d_1 = 10 cm

d)

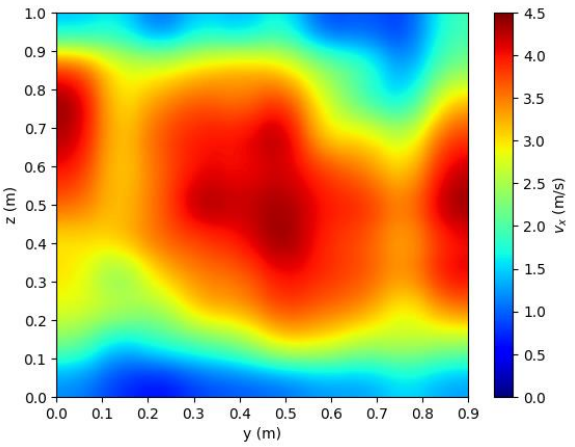

$\bar{v}_x = 2.9\ m/s$; d_1 = 10 cm

b)

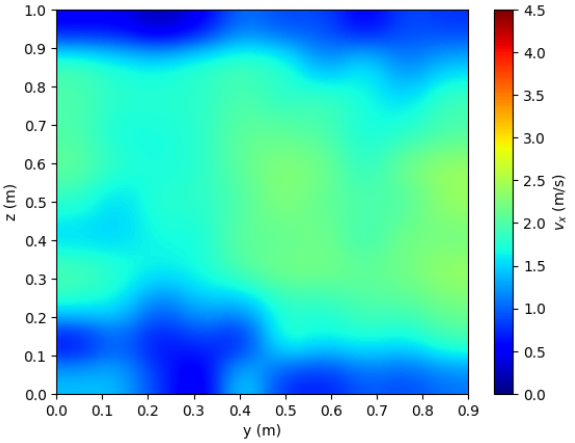

$\bar{v}_x = 1.6\ m/s$; d_2 = 20 cm

e)

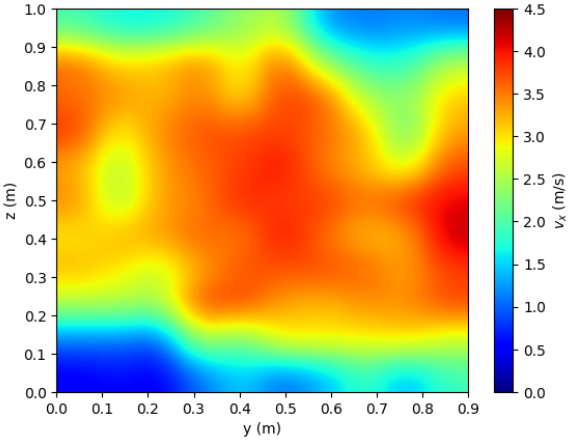

$\bar{v}_x = 2.9\ m/s$; d_2 = 20 cm

c)

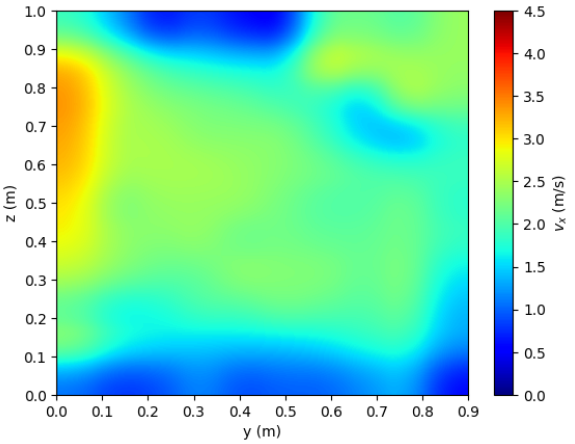

$\bar{v}_x = 2.0\ m/s$; d_3 = 40 cm

f)

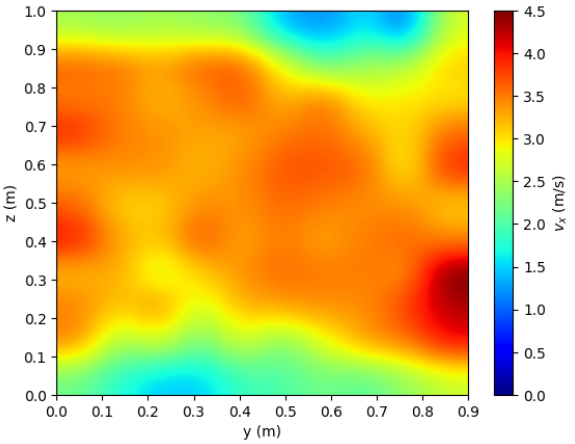

$\bar{v}_x = 3.1\ m/s$; d_3 = 40 cm

Figure 5: Velocity distribution on the suction side in front of the RT-HEX for a fan speed of 635 rpm (60 %) and for $d_1 – d_3$ on the left side a)-c) and for 1060 rpm (100 %) and for $d_1 – d_3$ on the right side d)-e).

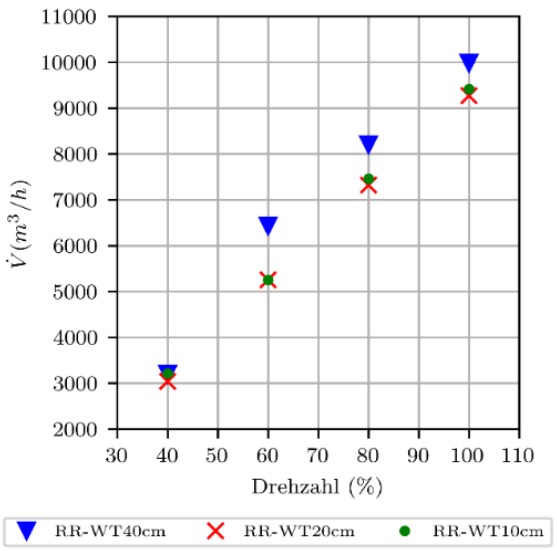

Figure 6: Flow rates depending on the fan speed and the distance between HEX and fan.

SIMULATION MODEL AND NUMERICAL SETUP

In order to speed up development processes and to reduce development costs, simulations become a more and more important tool in the product development process. Therefore, additionally to the experimental studies, simulations have been performed with a simplified model.

Heat exchanger model

For simplicity and to reduce computational costs, in the numerical simulations, the HEX is modeled as a porous medium. In the present studies, the pressure loss in the porous medium follows the Darcy-Forchheimer (DF) law [10, 11]. The DF law in Eqn. (2) describes this pressure loss depending on the inflow velocity:

$$\nabla p = -\mu A_i l\vec{u} - \frac{1}{2}\rho B_i l\vec{u}^2. \tag{2}$$

Where l is the thickness of the heat exchanger, $\vec{u}$ the velocity vector at the heat exchanger inlet, μ and ρ are the dynamic viscosity and the density of the ambient air. The constants A and B are determined by pressure measurements. To define the specific properties of the porous medium, the face velocity and the related pressure difference relative to the ambient air have been measured (see Figure 8a)). With the measured data, the two coefficients **A** and **B** and the individual DF laws for each HEX-fan configuration have been defined. For determining the DF laws with Eqn. (2), the averaged velocity $\bar{v}_x$ in flow direction was used, as illustrated in Figure 7 a). Initially, a simple test case was simulated to validate the Darcy-Forchheimer model. In this test case, the porous medium is placed in the center of a duct with slip walls, as depicted in Figure 7 b). As face velocity, the averaged velocity from the experimental studies measured in front of the HEX have been used (Figure 5). Figure 8 a) shows the simulated pressure loss in the duct with a DF law for d_3 and a fan speed of 635 rpm. The comparison between the measured and the simulated averaged pressure losses is presented in Figure 8 b). Fan speeds of 424 rpm (40 %), 635 rpm (60 %), 954 rpm (90 %) and 1060 rpm (100 %) are chosen as operating points. The crosses mark the measured and simulated results for the HEX-fan distance d_3 and the filled circles mark the simulated and measured pressure losses for d_1.

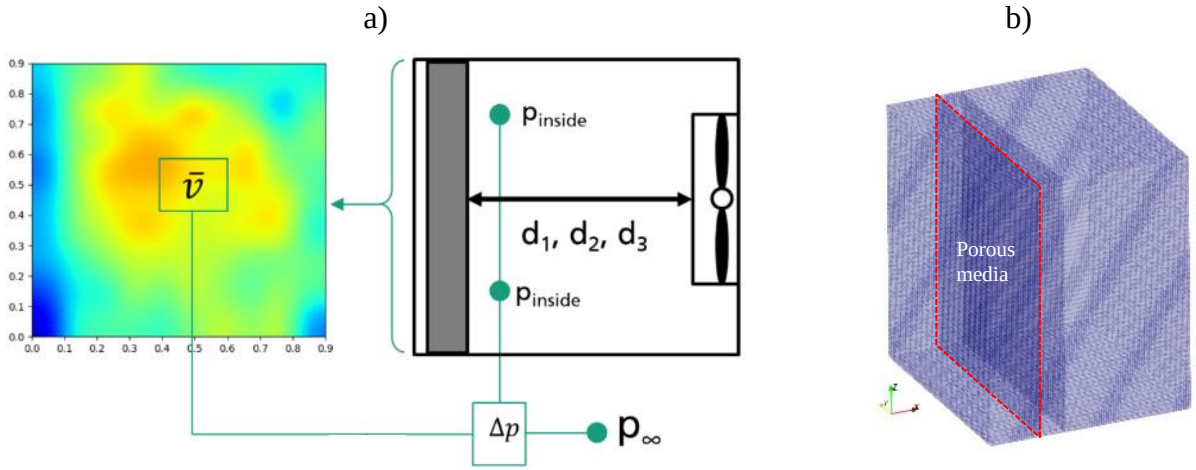

Figure 7: a) Schematic procedure to characterize the porous medium b) Simplified HEX model in a duct.

The diagram shows the pressure loss over the inflow velocity for various HEX-fan distances. The dashed lines represent the interpolated Darcy-Forchheimer curves, which are derived from the HEX models. The results in Figure 8 b) show that the trends found in the experiments can be reproduced in the simulations. A relatively good agreement is achieved for the results for d_1, with a maximum deviation between simulations and measurement of about 10 % at 1060 rpm. For d_3, the largest discrepancy between the simulations and measurements is found for 424 rpm with ca. 34 %. For higher fan speeds, the discrepancy remains below 15 %.

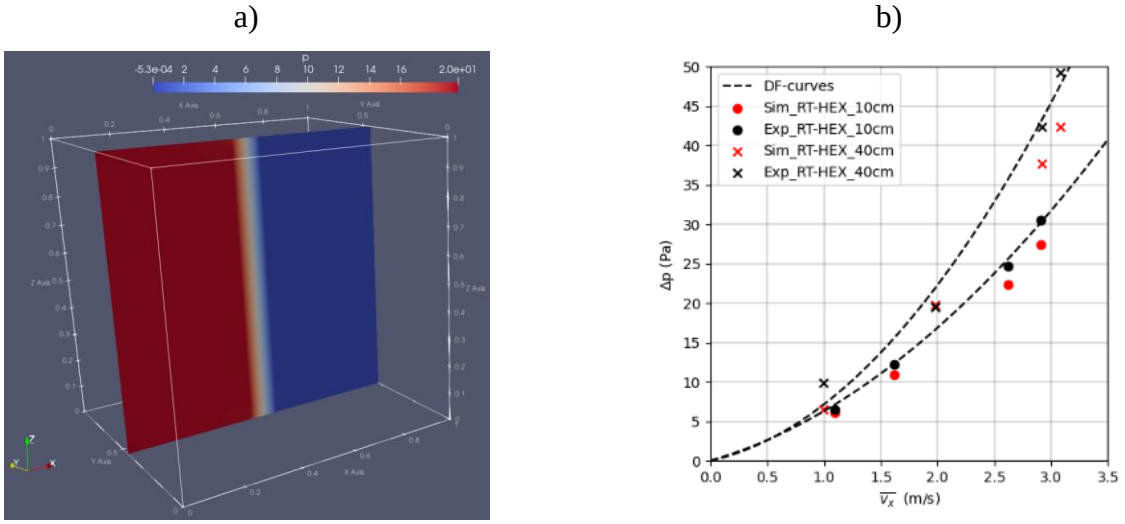

Figure 8: a) Test case to validate the Darcy-Forchheimer model and b) comparison between the measured and simulated pressure losses across the RT-HEX.

Heat pump model

In order to reduce the computational effort, a simplified CAD model of the heat pump mock-up is used in the numerical studies. The heat pump model is discussed in more detail in [3]. However, in addition to previous studies, a new CAD model of the fan is implemented, that is more similar to the geometry of the fan in the experimental mock-up. The model is depicted in Figure 9 a). All simulations are performed in OpenFOAM® v2006. The surface meshing is done in Salome v9.5.0. The volume mesh is generated with the meshing tools «blockMesh» and «snappyHexMesh»provided by OpenFOAM®. Due to limited computational resources, a steady-state simulation was performed for initialization with the «SIMPLE» algorithm [12]. In the steady-state simulations, the fan rotation is implemented using the Multi-Reference Frame technique with a rotation speed of 1060 rpm.

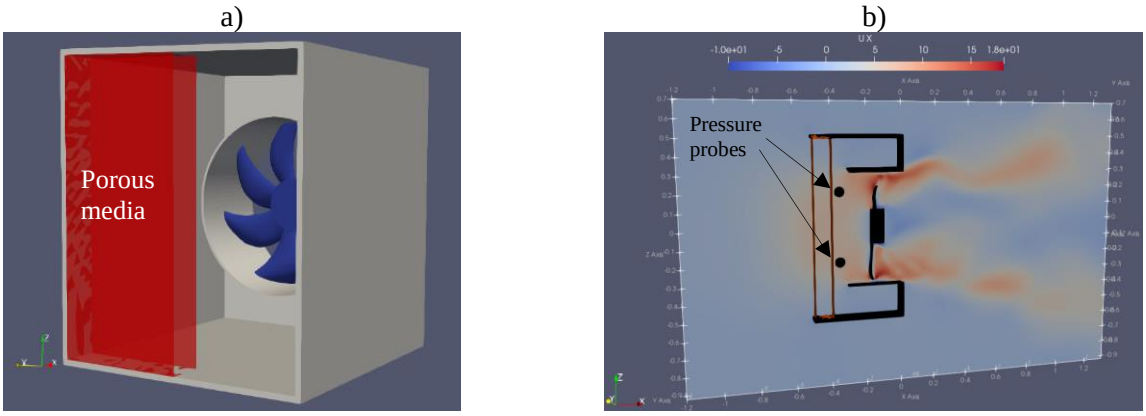

Figure 9: a) Heat pump model with porous medium as HEX and b) Flow field U_x indicating the location of the pressure probes.

In a second step, transient simulations have been performed with the «PIMPLE» algorithm [13] to calculate the velocity field. In the unsteady simulations, the fan rotation is simulated with an Arbitrary Mesh Interface (AMI). For the unsteady simulations, further refinements in the heat pump model as well as on the outflow side have been made, which result in a mesh with ca. 4 million cells. All simulations are performed considering air as incompressible fluid. For the turbulence modeling, the standard k-epsilon model is used. The ground below the heat pump geometry is defined as a rigid surface. For the boundary conditions on all the other sides, free outflow conditions are chosen, such as «pressureInletOutletVelocity» and a «total pressure» condition. Figure 9 b) shows the flow fields in U_x direction after a simulation time of t_{sim} = 2 s. The black points indicate the pressure probes where the pressure drop through the porous medium was measured in the simulation. The calculated averaged pressure loss in the simulations was ΔP = 30.2 Pa, which shows a good agreement with the experimental results presented in Figure 8 b). The simulations yield lower overall flow velocities compared to those measured experimentally.

CONCLUSION AND OUTLOOK

From the acoustic measurements presented in [3], it is clear that the sound pressure level of the BPF is influenced by the HEX-fan distance. To get a better understanding of this phenomenon, experimental and simulation studies have been performed on the flow velocity at the suction side in front of the HEX. The results of the experimental studies show that the flow rate increases with increasing distance between the HEX and the fan. For a fan speed of 635 rpm, the increase in the flow rate between configurations with d_1 = 10 cm and d_3 = 40 cm is about 25 %, and for 1060 rpm the difference is about 7 %. This may affect the heat transfer of the HEX and consequently also the COP of a heat pump. Furthermore, the larger change in the flow rate depending on the HEX-fan distance for lower fan speeds is identified as possible reason for the corresponding higher changes in the sound pressure levels around the BPF and its higher harmonics [3]. This, however, needs to be further investigated. Parallel to the acoustic and aerodynamic experiments, a simplified heat pump model has been created for aerodynamic and aeroacoustic simulations. In this paper, a heat pump model has been presented with an HEX modeled with the Darcy-Forchheimer law and an updated fan geometry. The surface-averaged pressure losses calculated with the Darcy-Forchheimer model show a relatively good agreement with the trends from the experiments. As a next step, the turbulence intensity determined through simulations with a submodel of the RT-HEX will be implemented in the settings of the porous medium properties. Additionally, aeroacoustic simulations will be performed with the updated model and a finer mesh to further investigate the influence of the HEX-fan distance. Furthermore, LDV measurements will be analyzed in more detail to gain a better understanding of the turbulence of the flow between the HEX and the fan and its effects on the noise emissions.

ACKNOWLEDGEMENT

This research has been conducted as part of the research project »WAMS«, which is funded by the German Federal Ministry for Economic Affairs and Energy (PTJ Förderkennzeichen 03ET1535A).

BIBLIOGRAPHY

[1] Umweltbundesamt: *Das Energie-Sparschwein*, **2013**

[2] REHVA: *European heat pump market*. REHVA Journal 04/2021, **2021**

[3] Wagner S., Adachi S., Rohlfing J.: *Experimental and numerical studies on the noise emissions from heat pumps, with respect to the heat exchanger - fan interaction. International Congress on Sound and Vibration,* **2020**

[4] OpenFOAM, www.openfoam.com (Accessed: 08.02.2022)

[5] Rathakrishnan, E.: *Instrumentation, Measurements, and Experiments in Fluids*. 2nd ed. Chapman and Hall/CRC, Boca Raton, **2016**.

[6] Zhang, Z.: *LDA Application Methods*. Springer, Berlin, Heidelberg, **2010**

[7] DIN 3741:2011-01: *Akustik- Bestimmung der Schallleistungs- und Schallenergiepegel von Geräuschquellen aus Schalldruckmessungen - Hallraumverfahren der Genauigkeitsklasse 1*. Beuth Verlag GmbH, Berlin, **2011**.

[8] Renz A., Zenger F., Becker S.: *Einfluss der Zuströmung auf das abgestrahlte Schallfeld von gesichelten Axialventilatoren*, DAGA, **2016**

[9] Czwielong F., Krömer F., Becker S.: *Experimental investigations of the sound emissons of axial fans under the influence of suction-side heat heat exchangers,* 25th AIAA/CEAS Aeroacoustics, *doi:*10.2514/6.2019-2618, **2019**

[10] OpenFOAMWiki, www.openfoamwiki.net/index.php/DarcyForchheimer (Accessed: 21.10.2021)

[11] Teng, H., Zhao, T.: *An extension of Darcy's law to non-Stokes flow in porous media*. Chemical Engineering Science, 14, S. 2727–2735, **2000**

[12] OpenFOAM User Guide: simpleFoam, www.openfoam.com/documentation/guides/latest/doc/guide-applications-solvers-incompressible-simpleFoam.html (Accessed: 06.04.2022)

[13] OpenFOAM User Guide: pimpleFoam, www.openfoam.com/documentation/guides/latest/doc/guide-applications-solvers-incompressible-pimpleFoam.html (Accessed: 06.04.2022)